Journal of Electronic Imaging

JElectronicImaging.org

Binary image deblurring with automatic binary value estimation

Xiao-Guang Lv
Fang Li

SPIE. IS&T imaging.org

Xiao-Guang Lv, Fang Li, "Binary image deblurring with automatic binary value estimation," *J. Electron. Imaging* **27**(3), 033043 (2018), doi: 10.1117/1.JEI.27.3.033043.

Binary image deblurring with automatic binary value estimation

Xiao-Guang Lv[a,b] and Fang Li[c,*]
[a]Huaihai Institute of Technology, School of Science, Lianyungang, China
[b]Nanjing Normal University, Jiangsu Key Laboratory for Numerical Simulation of Large Scale Complex Systems, Nanjing, China
[c]East China Normal University, School of Mathematical Sciences, Shanghai Key Laboratory of PMMP, Shanghai, China

Abstract. We propose a total variation-based variational model for nonblind binary image deblurring. The binary constraint is considered using the double-well function as the penalty term. We show the existence of a minimizer for the proposed model. By using operator splitting and alternating split Bregman, we get an effective numerical algorithm for the proposed model. Different from the existing methods in which the binary values are assumed to be known, our method can estimate the binary values automatically in the iteration process. Numerical results and comparisons demonstrate that the proposed algorithm is promising. *© 2018 SPIE and IS&T* [DOI: 10.1117/1.JEI.27.3.033043]

Keywords: total variation; binary image; double-well function; deblurring.

Paper 180202 received Mar. 7, 2018; accepted for publication Jun. 5, 2018; published online Jun. 28, 2018.

1 Introduction

The task of image deblurring is to recover a sharp image from its observed one that is corrupted by the blurring operator and additive noise. The blur arises from many sources such as an out-of-focus lens, atmosphere turbulence, relative movement between scene and camera, or object motion during exposure time.[1–5] The noise arises due to errors of the physical sensors or quantization in the image acquiring process. Mathematically, the image degradation model can be written as

$$g = Hf + \eta, \tag{1}$$

where g is the degraded image, f is the latent clean image, H is the spatial invariant blurring operator, and η is the additive Gaussian noise. In this paper, we focus on nonblind image deblurring, i.e., H is assumed to be known. The deblurring problem can be solved by the regularized least square model described as

$$\min_f \frac{1}{2}\int_\Omega |Hf - g|^2 \mathrm{d}x + \gamma J(f), \tag{2}$$

where $\Omega \subset \mathbb{R}^2$ is a bounded set, J is a regularizer, and γ is a positive regularization parameter. The widely used regularizers are sparsity priors including total variation (TV),[6,7] nonlocal total variation,[8,9] wavelet tight frames,[10,11] generalized Laplacian,[12] ℓ_0 norm,[13] and sorted ℓ_1.[14]

In this paper, we study the problem of recovering a binary image from its degraded observation. An image is binary if it has only two possible values for each pixel. Binary images are prevalent in digital systems and have a wide range of applications including texts, fingerprint recognition handwritten signatures, stellar astronomy, bar codes, and vehicle license plates.[15–17] There have been many attempts to deal with binary image deblurring. A straightforward approach is to treat the binary image as the gray-value image and postprocess it by thresholding. However, the drawback is that the thresholding step often destroys the structures in the recovered image. To enhance the binary image restoration quality, the prior information of being binary has been considered in a few works. Shen et al.[18] proposed a positive semidefinite programming approach for restoring the blurring and noisy binary image. Pan et al.[19] developed an effective ℓ_0 regularizer based on intensity and gradient prior for text image deblurring, which performs favorably against the existing text image deblurring methods. However, this prior might not be suitable for binary images with two values away from zero. Zhang[20] investigated the modification of the double-well function in order to guarantee the objective function to be convex. An alternating minimization algorithm is proposed to solve the binary image deblurring problem in which the Newton method is used to solve one of the subproblem inexactly. Mei et al.[21] proposed an effective second-order regularizer for the binary constraint. Both ℓ_0 regularization of gradient and TV are considered as image regularizers in their model. By operator splitting, the subproblem involving binary constraint can be solved exactly by soft-rounding. In addition, the statistical method was also employed for deblurring the binary image. Li and Lii[22] estimated the original image and the pixel values using the higher-order statistics.

A potential limitation of some existing methods such as Refs. 20 and 21 is that they assume that the two values of the latent binary image are known. To overcome this limitation, we propose a variational model for deblurring the binary image with unknown pixel values. The proposed model is based on the TV regularization of image and the double-well function for binary constraint. Mathematically, we prove the existence of minimizer for the proposed model. We use the operator splitting scheme and the alternating split Bregman (ASB) method to derive an efficient algorithm in

*Address all correspondence to: Fang Li, E-mail: fli@math.ecnu.edu.cn

which each subproblem has closed-form solution. Especially, the binary values can be estimated automatically in the iteration process.

2 Proposed Model and Mathematical Analysis

In this paper, we propose to use the double-well function as a regularizer for binary constraint which is defined as

$$\phi_1(z) = (z-\beta_1)^2(z-\beta_2)^2, \qquad z \in \mathbb{R}.$$

For comparison, we recall two closely related functions that were used in Refs. 20 and 21

$$\phi_2(z) = \begin{cases} (z-\beta_1)^2(z-\beta_2)^2, & z < \beta_1 \text{ or } z > \beta_2, \\ 0, & \beta_1 \le z \le \beta_2 \end{cases}$$

$$\phi_3(z) = \begin{cases} \beta_1 - z, & z < \beta_1 \\ (z-\beta_1)(\beta_2 - z), & \beta_1 \le z \le \beta_2 \\ z - \beta_2, & z > \beta_2 \end{cases}.$$

In Fig. 1, we plot the three functions with $\beta_1 = 0$ and $\beta_2 = 1$.

Obviously, the double-well regularizer $\phi_1(z)$ and the soft-rounding regularizer $\phi_3(z)$ are nonconvex and they attain their minimum at 0 and 1. Compared with the soft-rounding regularizer $\phi_3(z)$, the double-well regularizer $\phi_1(z)$ is smooth. Optimization problems involving smooth functions are much easier and more convenient to be solved. The regularizer $\phi_2(z)$ is a convex version of $\phi_1(z)$. Although $\phi_2(z)$ is convex, its drawback is that it relaxes $z \in [\beta_1, \beta_2]$ which makes z very far from binary. Compared with the convex regularizer $\phi_2(z)$, the double-well regularizer $\phi_1(z)$ can force the pixel values of the recovered image to approach zero and one better.

Assume $g: \Omega \to \mathbb{R}^2$ is the observed image where $\Omega \subset \mathbb{R}^2$ is a bounded set with the Lipschitz boundary. In this paper, we propose the following variational model for binary image deblurring:

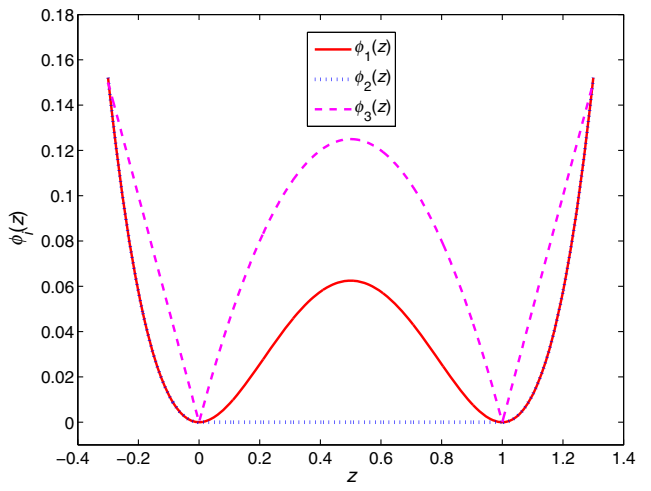

Fig. 1 The binary regularizers. The red solid line shows our double-well regularizer $\phi_1(x)$, the blue dotted line shows the regularizer $\phi_2(x)$ in Ref. 20, and the magenta dashed line shows the regularizer $\phi_3(x)$ in Ref. 21.

$$\inf_{f,\beta_1,\beta_2} \left\{ \begin{array}{l} E(f,\beta_1,\beta_2) = \frac{1}{2}\int_\Omega |Hf-g|^2 \mathrm{d}x \\ +\frac{\alpha}{2}\int_\Omega (f-\beta_1)^2(f-\beta_2)^2 \mathrm{d}x + \gamma J(f) \end{array} \right\}, \tag{3}$$

where α and γ are positive regularization parameters, β_1 and β_2 are the pixel values to be estimated, and $J(f)$ is the TV seminorm defined as

$$J(f) = \sup\{f \mathrm{div}(\xi)\mathrm{d}x / \xi(x) \in C_0^\infty(\Omega, \mathbb{R}^2), |\xi| \le 1\}.$$

In the energy functional of Eq. (3), the first term is the data fitting term, the second term is the double-well function which acts as a binary regularizer and forces pixel values of the recovered image to approach β_1 and β_2, and the last term is the TV regularizer which is especially suitable for piecewise constant images including binary images.[6,23]

Note that the optimization Eq. (3) is nonconvex and involves three set of variables. In the following, we show that if f is bounded, the optimization Eq. (3) has at least one solution (f, β_1, β_2) such that $f \in BV(\Omega)$. Here $BV(\Omega)$ is the bounded variation space which is the subspace of functions $u \in L^2(\Omega)$ with bounded TV.

Theorem 1 Assume $H: L^2(\Omega) \to L^2(\Omega)$ is a linear continuous operator. Let the given image $g \in L^2(\Omega)$, if $a_1 \le f \le a_2$, then the optimization Eq. (3) has at least one solution $(f_*, \beta_{1*}, \beta_{2*})$ such that $f_* \in BV(\Omega)$, $a_1 \le f_* \le a_2$, $a_1 \le \beta_{1*} \le a_2$ and $a_1 \le \beta_{2*} \le a_2$.

Proof 1 Let $f \equiv a_1$, $\beta_1 \equiv a_1$, $\beta_2 \equiv a_2$, we have $E(a_1, a_1, a_2) = \frac{1}{2}\int_\Omega (Ha_1 - g)^2 \mathrm{d}x$. Since $g \in L^2(\Omega)$ and Ω are bounded, $E(a_1)$ is finite. Hence the infimum of the energy must be finite. Let us consider a minimizing sequence $\{f_n, \beta_{1n}, \beta_{2n}\}$ for the energy of Eq. (3) which satisfies $f_n \in BV(\Omega)$, $a_1 \le f_n \le a_2$, that is, $E(f_n, \beta_{1n}, \beta_{2n}) \to \inf E(f, \beta_1, \beta_2)$ as $n \to \infty$. Then, we have

$$E(f_n, \beta_{1n}, \beta_{2n}) = \frac{1}{2}\int_\Omega |Hf_n - g|^2 \mathrm{d}x + \frac{\alpha}{2}\int_\Omega (f_n - \beta_{1n})^2(f_n - \beta_{2n})^2 \mathrm{d}x + \gamma J(f_n) < C,$$

where $C > 0$ is a constant. Therefore, we have that $J(f_n)$ is uniformly bounded. Meanwhile, $a_1 \le f_n \le a_2$ implies that $\|f_n\|_{L^1(\Omega)}$ is uniformly bounded. Hence, we get that $\{f_n\}$ is uniformly bounded in $BV(\Omega)$. By using the compactness property of BV space with to weak * topology, up to a subsequence also denoted by $\{f_n\}$, there exists a function $f_* \in BV(\Omega)$ which satisfies $a_1 \le f_* \le a_2$ such that

$$f_n \to f_* \text{ strongly in } L^1(\Omega),$$
$$f_n \to f_* \quad \text{a.e. } x \in \Omega,$$
$$Df_n \rightharpoonup Df_* \text{ in the sense of measure.}$$

Then by the lower semicontinuity of L^2 norm and TV, we get

$$\int_\Omega |Hf_* - g|^2 \mathrm{d}x \le \lim_{n\to\infty} \inf \int_\Omega |Hf_n - g|^2 \mathrm{d}x, \tag{4}$$

$$J(f_*) \le \lim_{n\to\infty} \inf J(f_n). \tag{5}$$

On the other hand, we can derive from the energy model Eq. (3) that the sequences $\{\beta_{1n}\}$ and $\{\beta_{2n}\}$ satisfy the following first-order optimal conditions:

$$\int_\Omega (f_n-\beta_{1n})(f_n-\beta_{2n})^2 \mathrm{d}x = 0,$$
$$\int_\Omega (f_n-\beta_{2n})(f_n-\beta_{1n})^2 \mathrm{d}x = 0.$$

The solution is given as

$$\beta_{1n}=\frac{\int_\Omega f_n(f_n-\beta_{2n})^2\mathrm{d}x}{\int_\Omega (f_n-\beta_{2n})^2\mathrm{d}x}, \qquad \beta_{2n}=\frac{\int_\Omega f_n(f_n-\beta_{1n})^2\mathrm{d}x}{\int_\Omega (f_n-\beta_{1n})^2\mathrm{d}x}.$$

It is easy to see that $a_1 \le \beta_{in} \le a_2$, $i=1,2$. Hence up to subsequences, also denoted by $\{\beta_{1n}\}$ and $\{\beta_{2n}\}$, there exist β_{1*} and β_{2*} such that

$$\beta_{1n}\to\beta_{1*}\in[a_1,a_2], \qquad \beta_{2n}\to\beta_{2*}\in[a_1,a_2].$$

Then $(f_n-\beta_{1n})^2(f_n-\beta_{2n})^2 \to (f_*-\beta_{1*})^2(f_*-\beta_{2*})^2$ a.e. $x\in\Omega$. By the Fotou lemma, we get

$$\int_\Omega (f_*-\beta_{1*})^2(f_*-\beta_{2*})^2\mathrm{d}x \le \liminf_{n\to\infty}\int_\Omega (f_n-\beta_{1n})^2(f_n-\beta_{2n})^2\mathrm{d}x. \tag{6}$$

Summing up Eqs. (4)–(6), we get

$$E(f_*,\beta_{1*},\beta_{2*}) \le \liminf_{n\to\infty} E(f_n) = \inf\ E(f). \tag{7}$$

Hence $(f_*,\beta_{1*},\beta_{2*})$ must be a minimizer of the optimization Eq. (3) satisfying $f_*\in BV(\Omega)$ and $a_1\le f_*\le a_2$. This completes the proof.

It should be noted that in Theorem 1, we assume $f\in[a_1,a_2]$. The bounded condition is often satisfied in the practical problems. Hence, this assumption can be removed in the proposed model and the corresponding numerical scheme.

3 Algorithm

The proposed minimization Eq. (3) is difficult to solve directly since it is nonconvex, nonsmooth, and contains a fourth-order polynomial. In order to solve it efficiently, we use the popular operator splitting scheme and the ASB method. It has been proved in Ref. 24 that ASB is equivalent to the classical alternating direction method of multipliers.

Note that in the numerical implementation, the TV of f is equivalent to the L^1 norm of the gradient of f, that is, $J(f)=\|\nabla f\|_1$. Then we can rewrite the proposed model Eq. (3) as

$$\min_{f,\beta_1,\beta_2}\frac{1}{2}\|Hf-g\|_2^2+\frac{\alpha}{2}\int_\Omega (f-\beta_1)^2(f-\beta_2)^2\mathrm{d}x+\gamma\|\nabla f\|_1. \tag{8}$$

First, we introduce three auxiliary variables and rewrite model Eq. (8) as the following equivalent formulation with constraints:

$$\min_{f,\beta_1,\beta_2}\frac{1}{2}\|Hf-g\|_2^2+\frac{\alpha}{2}\int_\Omega (u-\beta_1)^2(v-\beta_2)^2\mathrm{d}x+\gamma\|w\|_1 \quad \text{s.t. } f=u,\quad f=v,\quad \nabla f=w. \tag{9}$$

Following the framework of ASB, we define the function $\mathcal{L}(f,\beta_1,\beta_2,u,v,w)$ as

$$\mathcal{L}=\left\{\begin{array}{l}\frac{1}{2}\|Hf-g\|_2^2+\frac{\alpha}{2}\int_\Omega (u-\beta_1)^2(v-\beta_2)^2\mathrm{d}x+\gamma\|w\|_1\\ +\frac{\sigma_1}{2}\|f-u+b\|_2^2+\frac{\sigma_2}{2}\|f-v+c\|_2^2+\frac{\sigma_3}{2}\|\nabla f-w+d\|_2^2\end{array}\right\}, \tag{10}$$

where b, c, d are the Lagrangian multipliers and σ_i $(i=1,\ 2,\ 3)$ are the penalty parameters.[25] In fact, $\mathcal{L}(f,\beta_1,\beta_2,u,v,w)$ is equivalent to the augmented Lagrangian of the original constrained Eq. (9). Then the ASB method for the minimization Eq. (9) is given by the following iteration scheme:

$$f^{k+1}=\arg\min_f \mathcal{L}(f,\beta_1^k,\beta_2^k,u^k,v^k,w^k), \tag{11}$$

$$\beta_1^{k+1}=\arg\min_{\beta_1} \mathcal{L}(f^{k+1},\beta_1,\beta_2^k,u^k,v^k,w^k), \tag{12}$$

$$\beta_2^{k+1}=\arg\min_{\beta_2} \mathcal{L}(f^{k+1},\beta_1^{k+1},\beta_2,u^k,v^k,w^k), \tag{13}$$

$$u^{k+1}=\arg\min_u \mathcal{L}(f^{k+1},\beta_1^{k+1},\beta_2^{k+1},u,v^k,w^k), \tag{14}$$

$$v^{k+1}=\arg\min_v \mathcal{L}(f^{k+1},\beta_1^{k+1},\beta_2^{k+1},u^{k+1},v,w^k), \tag{15}$$

$$w^{k+1}=\arg\min_w \mathcal{L}(f^{k+1},\beta_1^{k+1},\beta_2^{k+1},u^{k+1},v^{k+1},w). \tag{16}$$

In the following, we give the solutions of Eqs. (11)–(16). The first subproblem corresponds to the following optimization problem:

$$\arg\min_f \frac{1}{2}\|Hf-g\|_2^2+\frac{\sigma_1}{2}\|f-u^k+b^k\|_2^2 +\frac{\sigma_2}{2}\|f-v^k+c^k\|_2^2+\frac{\sigma_3}{2}\|\nabla f-w^k+d^k\|_2^2. \tag{17}$$

The minimizer can be obtained by equivalently solving a linear system

$$(H^TH+\sigma_1 I+\sigma_2 I+\sigma_3\nabla^T\nabla)f = H^Tg+\sigma_1(u^k-b^k)+\sigma_2(v^k-c^k)+\sigma_3\nabla^T(w^k-d^k). \tag{18}$$

Note that K, ∇ have block circulant with circulant blocks (BCCB) structure when the periodic boundary conditions are used. We know that the computations with BCCB matrices can be very efficient using fast Fourier transforms (FFTs). Let $\mathcal{F}$ denote the FFT. We have

$$f^{k+1}=\mathcal{F}^{-1}\left\{\frac{\mathcal{F}[H^Tg+\sigma_1(u^k-b^k)+\sigma_2(v^k-c^k)+\sigma_3(w^k-d^k)]}{\mathcal{F}(H^TH+\sigma_1I+\sigma_2I+\sigma_3\nabla^T\nabla)}\right\}. \tag{19}$$

As for β_1 and β_2, we have

$$\beta_1^{k+1}=\arg\min_{\beta_1}\frac{\alpha}{2}\int_\Omega(u^k-\beta_1)^2(v^k-\beta_2^k)^2\mathrm{d}x \tag{20}$$

and

$$\beta_2^{k+1}=\arg\min_{\beta_1}\frac{\alpha}{2}\int_\Omega(u^k-\beta_1^{k+1})^2(v^k-\beta_2)^2\mathrm{d}x. \tag{21}$$

Taking the derivatives with respect to β_1 and β_2, respectively, and setting the results to be zero, we get

$$\alpha\int_\Omega(u^k-\beta_1)(v^k-\beta_2^k)^2=0, \tag{22}$$

and

$$\alpha\int_\Omega(u^k-\beta_1^{k+1})^2(v^k-\beta_2)=0. \tag{23}$$

So we have

$$\beta_1^{k+1}=\frac{\int_\Omega u^k(v^k-\beta_2^k)^2\mathrm{d}x}{\int_\Omega(v^k-\beta_2^k)^2\mathrm{d}x} \tag{24}$$

and

$$\beta_2^{k+1}=\frac{\int_\Omega v^k(u^k-\beta_1^{k+1})^2\mathrm{d}x}{\int_\Omega(u^k-\beta_1^{k+1})^2\mathrm{d}x}. \tag{25}$$

For u and v, we have

$$u^{k+1}=\arg\min_u\frac{\alpha}{2}\int_\Omega(u-\beta_1^{k+1})^2(v^k-\beta_2^{k+1})^2\mathrm{d}x+\frac{\sigma_1}{2}\|f^{k+1}-u+b^k\|_2^2 \tag{26}$$

and

$$v^{k+1}=\arg\min_v\frac{\alpha}{2}\int_\Omega(u^{k+1}-\beta_1^{k+1})^2(v-\beta_2^{k+1})^2\mathrm{d}x+\frac{\sigma_2}{2}\|f^{k+1}-v+c^k\|_2^2. \tag{27}$$

So the minimizers u^{k+1} and v^{k+1} can be easily obtained as

$$u^{k+1}=\frac{\alpha\beta_1^{k+1}(v^k-\beta_2^{k+1})^2+\sigma_1(f^{k+1}+b^k)}{\alpha(v^k-\beta_2^{k+1})^2+\sigma_1} \tag{28}$$

and

$$v^{k+1}=\frac{\alpha\beta_2^{k+1}(u^{k+1}-\beta_1^{k+1})^2+\sigma_2(f^{k+1}+c^k)}{\alpha(u^{k+1}-\beta_1^{k+1})^2+\sigma_2}. \tag{29}$$

Algorithm 1 Binary image deblurring with automatic binary value estimation.

- Initialization: $f^0=g$, $\beta_1^0=0$, $\beta_2^0=0$, $u^0=g$, $v^0=g$, $w^0=\nabla f$, $b^0=0$, $c^0=0$, $d^0=0$.
- For $k=0,1,2,\ldots$, repeat until stopping criterion is reached

$$f^{k+1}=\mathcal{F}^{-1}\left\{\frac{\mathcal{F}[H^Tg+\sigma_1(u^k-b^k)+\sigma_2(v^k-c^k)+\sigma_3(w^k-d^k)]}{\mathcal{F}(H^TH+\sigma_1I+\sigma_2I+\sigma_3\nabla^T\nabla)}\right\},$$
$$\beta_1^{k+1}=\frac{\int_\Omega u^k(v^k-\beta_2^k)^2\mathrm{d}x}{\int_\Omega(v^k-\beta_2^k)^2\mathrm{d}x},$$
$$\beta_2^{k+1}=\frac{\int_\Omega v^k(u^k-\beta_1^{k+1})^2\mathrm{d}x}{\int_\Omega(u^k-\beta_1^{k+1})^2\mathrm{d}x},$$
$$u^{k+1}=\frac{\alpha\beta_1^{k+1}(v^k-\beta_2^{k+1})^2+\sigma_1(f^{k+1}+b^k)}{\alpha(v^k-\beta_2^{k+1})^2+\sigma_1},$$
$$v^{k+1}=\frac{\alpha\beta_2^{k+1}(u^{k+1}-\beta_1^{k+1})^2+\sigma_2(f^{k+1}+c^k)}{\alpha(u^{k+1}-\beta_1^{k+1})^2+\sigma_2},$$
$$w^{k+1}=\mathcal{S}(\nabla f^{k+1}+d^k,\gamma/\sigma_3),$$
$$b^{k+1}=b^k+f^{k+1}-u^{k+1},$$
$$c^{k+1}=c^k+f^{k+1}-v^{k+1},$$
$$d^{k+1}=d^k+\nabla f^{k+1}-w^{k+1}.$$

- Output: f^{k+1}, β_1^{k+1}, β_2^{k+1}

As for w, we have

$$w^{k+1} = \arg\min_{w} \gamma\|w\|_1 + \frac{\sigma_3}{2}\|\nabla f^{k+1} - w + d^k\|_2^2. \tag{30}$$

The minimizer is given by the following soft shrinkage equation:

$$w^{k+1} = \mathcal{S}(\nabla f^{k+1} + d^k, \gamma/\sigma_3), \tag{31}$$

where the soft shrinkage operator is defined as

$$\mathcal{S}(t,\tau) \coloneqq \max(|t| - \tau, 0)\operatorname{sign}(t) = \arg\min_{s} \tau\|s\|_1 + \frac{1}{2}\|s - t\|_2^2. \tag{32}$$

The updating scheme of the Lagrangian multipliers can be written specifically as

$$\begin{aligned} b^{k+1} &= b^k + f^{k+1} - u^{k+1}, \\ c^{k+1} &= c^k + f^{k+1} - v^{k+1}, \\ d^{k+1} &= d^k + \nabla f^{k+1} - w^{k+1}. \end{aligned} \tag{33}$$

The final numerical scheme for the proposed model is summarized in Algorithm 1.

4 Numerical Results

In this section, we give some numerical tests to illustrate the effectiveness of the proposed method for binary image deblurring. We compare the proposed method with some existing deblurring methods including the classical TV method in Ref. 26, the l_0 regularized intensity and gradient prior method (l_0) in Ref. 19, the alternating minimization method (AM) in Ref. 20, and the soft rounding-based method (SR) in Ref. 21. In order to have fair comparisons in all tests, we adjust parameters and report the best overall performance for the five methods.

We use the stopping criterion when the maximum number of allowed outer iterations $N = 500$ has been carried out or the relative differences between consecutive iterates $f^1, f^2, f^3, \ldots$ satisfy

$$\frac{\|f^{k+1} - f^k\|_2}{\|f^{k+1}\|_2} < 10^{-5}.$$

Table 1 Test on "barcode" image: estimation capabilities of $\{\beta_1, \beta_2\}$.

Noise	Blur	True = {0, 1}	True = {−1, 1}
1%	Gauss	{0.0000, 1.0000}	{−1.0014, 1.0009}
	Defocus	{0.0000, 1.0000}	{−1.0015, 1.0013}
	Motion	{0.0000, 1.0000}	{−0.9996, 0.9996}
2%	Gauss	{0.0000, 1.0000}	{−1.0002, 1.0015}
	Defocus	{−0.0006, 1.0002}	{−1.0006, 1.0011}
	Motion	{0.0000, 0.9999}	{−0.9994, 0.9994}
3%	Gauss	{0.0000, 0.9995}	{−1.0007, 0.9967}
	Defocus	{0.0000, 0.9995}	{−1.0005, 0.9978}
	Motion	{0.0001, 0.9997}	{−1.0000, 0.9971}
4%	Gauss	{0.0001, 0.9996}	{−1.0003, 1.0023}
	Defocus	{0.0002, 0.9999}	{−1.0001, 1.0013}
	Motion	{0.0002, 0.9996}	{−0.9986, 0.9987}
5%	Gauss	{0.0002, 0.9991}	{−1.0000, 1.0020}
	Defocus	{−0.0006, 0.9995}	{−0.9999, 1.0008}
	Motion	{0.0003, 0.9994}	{−0.9982, 0.9983}
6%	Gauss	{0.0001, 0.9988}	{−0.9999, 1.0017}
	Defocus	{−0.0008, 0.9998}	{−0.9991, 1.0007}
	Motion	{0.0001, 0.9994}	{−0.9979, 0.9983}

In the iteration process, we increase the parameter α to two times every 30 iterations for speeding up convergence. In the experiments, we apply three kinds of commonly used PSFs generated by the MATLAB routines: (i) fspecial ("Gaussian,"11,5), the 11×11 Gaussian blur with standard deviation 5; (ii) fspecial("disk,"5), the out-of-focus (defocus) blur with size 11×11; (iii) fspecial("motion,"7,45), the

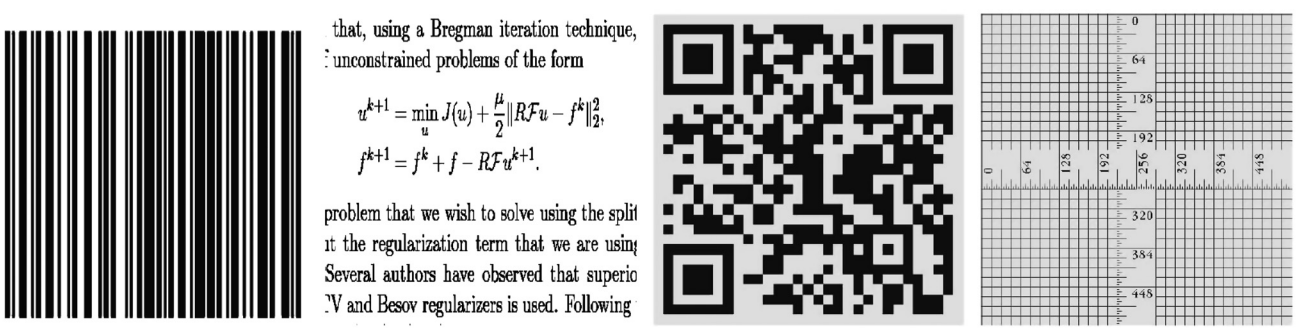

(a) (b) (c) (d)

Fig. 2 Test images. (a) Barcode, (b) text, (c) QR code, and (d) ruler.

motion blur with size 7×7. To evaluate the quality of the restoration results quantitatively, we use the peak signal-to-noise ratio (PSNR) and structural similarity index (SSIM). See Ref. 27 for more details. Four test images "barcode," "text," "quick response (QR) code," and "ruler" are shown in Fig. 2.

In the first test, we show the estimation capabilities of β_1 and β_2 and the convergence behavior of the proposed method. In this test, we compute β_1 and β_2 using the proposed method when the true pixel values $\{\beta_1, \beta_2\}$ of the binary image "barcode" in Fig. 2 are $\{0, 1\}$ and $\{-1, 1\}$, respectively. The estimated pixel values produced by the proposed method are given under the three different blurs and six noise levels in Table 1. The noise level is defined by $\frac{\|\eta\|_2}{\|Hf\|_2}$. It is easy to see from the table that our method has a strong binary value estimation ability for 1% to 6% noise levels. Especially, we can estimate the values exactly under the 1% noise level when the true pixel values are $\{0, 1\}$. In Fig. 3, we plot the numerical convergence results of

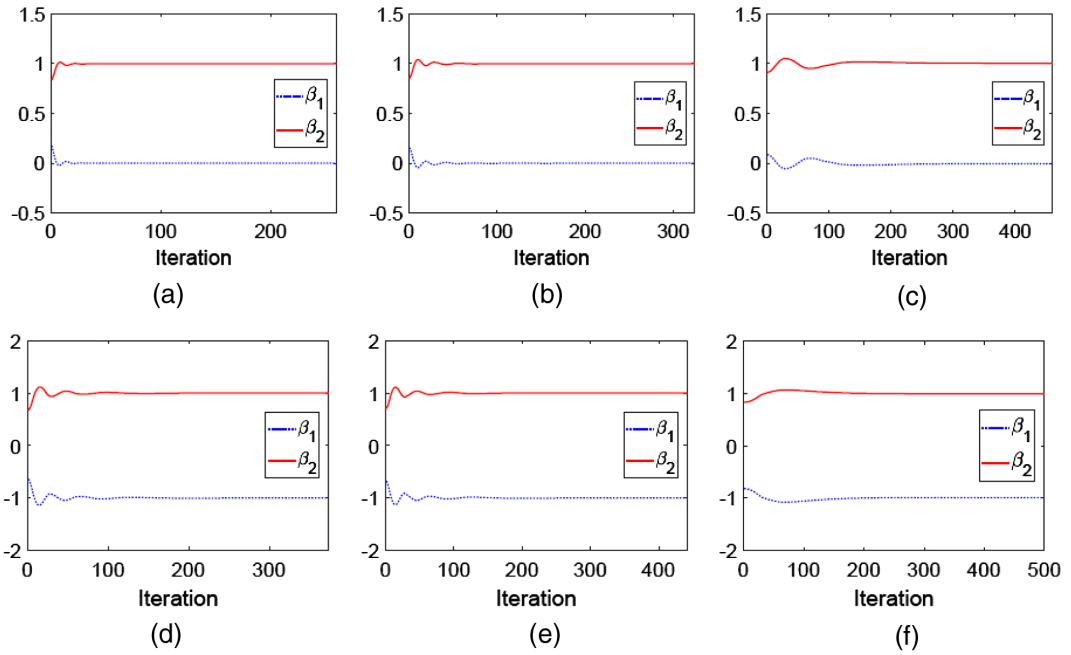

Fig. 3 Convergence behavior of β_1 and β_2. (a) Gauss, 1% noise, (b) defocus, 2% noise, (c) motion, 3% noise, (d) Gauss, 4% noise, (e) defocus, 5% noise, and (f) motion, 6% noise.

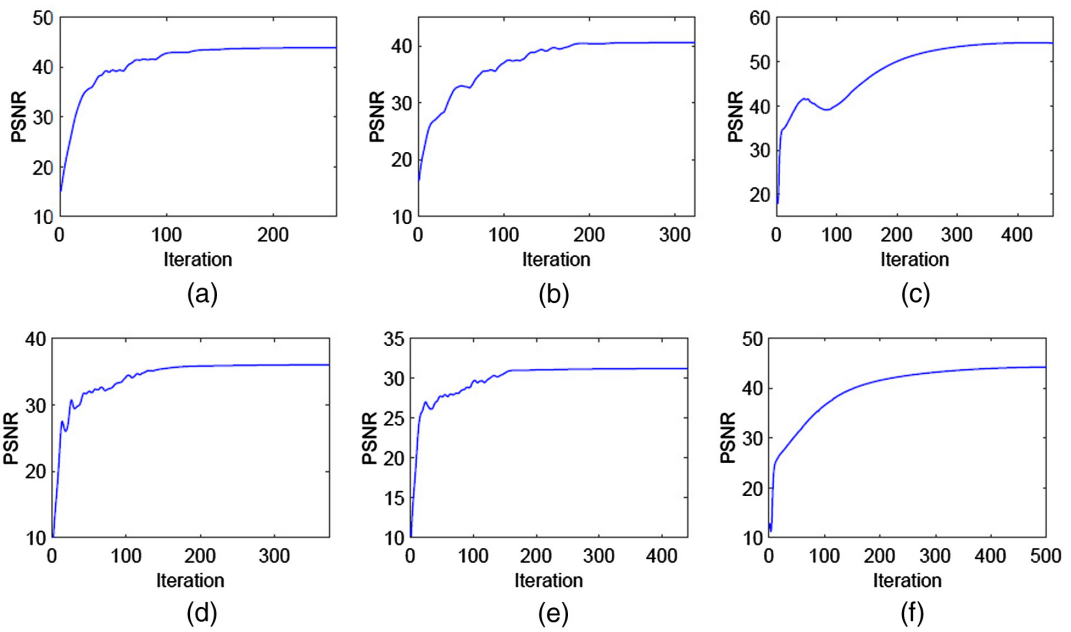

Fig. 4 Convergence behavior of the estimated image. (a) Gauss, 1% noise, (b) defocus, 2% noise, (c) motion, 3% noise, (d) Gauss, 4% noise, (e) defocus, 5% noise, and (f) motion, 6% noise.

the binary pixel values $\{\beta_1, \beta_2\}$ for 1% to 6% noise levels. The true pixel values of the first row in Fig. 3 are 0 and 1 while the true pixel values of the second row are -1 and 1. As can be seen from Fig. 3, the iteration sequences about the estimated pixel values are convergent. To show the convergence behavior of our method for binary image deblurring, we report the PSNR values of the restored images for each iteration in Fig. 4. It is not difficult to see from the figure that the proposed method is numerically convergent.

In the second test, we compare the restoration results by TV, l_0, and the proposed method when the pixel values of the binary image are unknown. In Table 2, we give the PSNR and SSIM results for TV, l_0, and the proposed method. Note that in Table 2 the best results are marked in bold. From the table, we know that our method behaves much better in terms of PSNR and SSIM. We show the resorted binary images for "text" under the Gaussian blur and 1% noise level in Fig. 5 while the motion blur and 6% noise level in Fig. 6. It is not difficult to see from the visual quality of restored images in the figures that the proposed method is better than the other methods. See the marked rectangles for a better visual comparison.

In the third test, we compare the restoration results when the pixel values of the binary images are known. The pixel values of the two images "QR barcode" and "tuler" are known to be 16 and 224. In Table 3, we report the PSNR and SSIM values by AM, SR, and the proposed method under three different blurs and 1% to 6% noise levels for "QR code" and "ruler" images, respectively. We observe from Table 3 that the PSNR and SSIM values obtained by the proposed method are the highest among the three methods. Especially, under the Gaussian and motion blurs with 1% and 3% noise levels, respectively, our method recovers the original image "QR code" exactly. In Figs. 7 and 8, we display the restoration results when AM, SR, and the

Table 2 Test on "text" image: comparison of the performance for unknown binary pixel values.

	Blur	Gauss	Defocus	Motion
	Noise	1%	2%	3%
PSNR	TV[26]	11.43	14.40	20.14
	l_0[19]	11.99	17.30	27.14
	Ours	**16.37**	**25.99**	**45.23**
SSIM	TV[26]	0.8433	0.7750	0.8828
	l_0[19]	0.8937	0.9641	0.9861
	Ours	**0.9529**	**0.9914**	**0.9880**
	Noise	4%	5%	6%
PSNR	TV[26]	9.31	10.26	15.33
	l_0[19]	9.70	10.42	20.67
	Ours	**10.13**	**11.53**	**34.84**
SSIM	TV[26]	0.7826	0.8118	0.9772
	l_0[19]	0.7820	0.7977	0.9813
	Ours	**0.7826**	**0.8246**	**0.9995**

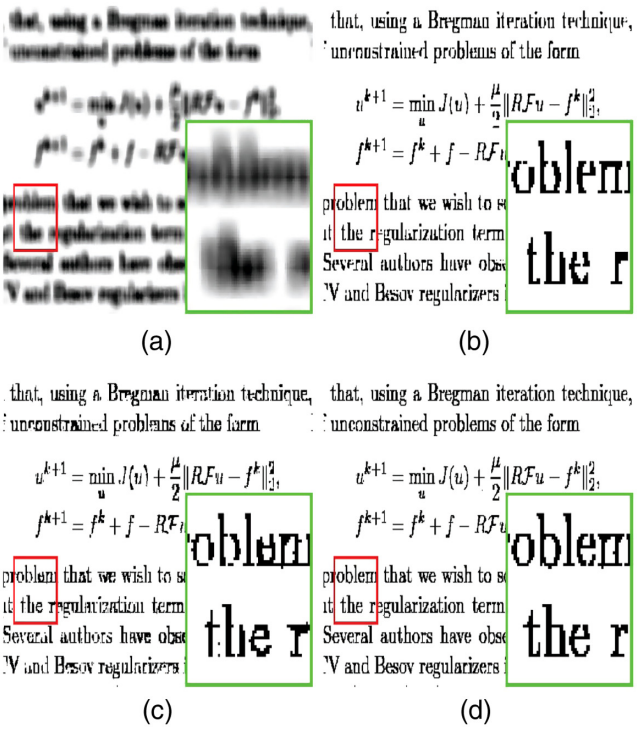

Fig. 5 Restoration results for unknown binary pixel values (Gauss, 1% noise). (a) Degraded, (b) TV,[26] (c) l_0,[19] and (d) ours.

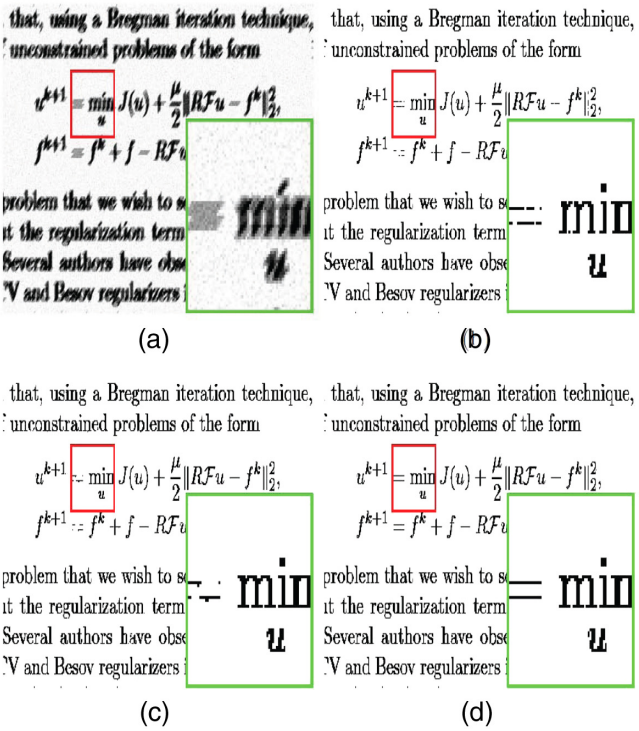

Fig. 6 Restoration results for unknown binary pixel values (motion, 6% noise). (a) Degraded, (b) TV,[26] (c) l_0,[19] and (d) ours.

Table 3 Test on "QR code" and "ruler" images: comparison of the performance for known binary pixel values.

Image	Blur		Gauss	Defocus	Motion
	Noise		1%	2%	3%
QR code	PSNR	AM[20]	37.38	33.60	49.93
		SR[21]	45.16	39.93	**inf**
		Ours	**inf**	**42.94**	**inf**
	SSIM	AM[20]	0.9670	0.9945	0.9999
		SR[21]	0.9999	0.9989	**1.0000**
		Ours	**1.0000**	**0.9996**	**1.0000**
Ruler	PSNR	AM[20]	25.30	17.64	27.67
		SR[21]	27.41	18.82	28.12
		Ours	**27.68**	**19.29**	**30.97**
	SSIM	AM[20]	0.9871	0.9245	0.9931
		SR[21]	0.9936	0.9474	0.9941
		Ours	**0.9937**	**0.9539**	**0.9966**
		Noise	4%	5%	6%
QR code	PSNR	AM[20]	23.14	25.21	30.54
		SR[21]	24.87	25.27	32.28
		Ours	**26.61**	**28.03**	**36.32**
	SSIM	AM[20]	0.9542	0.9670	0.9917
		SR[21]	0.9765	0.9735	0.9946
		Ours	**0.9766**	**0.9845**	**0.9980**
Ruler	PSNR	AM[20]	13.75	13.69	17.19
		SR[21]	14.15	13.93	17.38
		Ours	**14.61**	**14.15**	**19.58**
	SSIM	AM[20]	0.6559	0.7343	0.8909
		SR[21]	0.7963	0.7353	0.8942
		Ours	**0.8066**	**0.7478**	**0.9535**

Note: The best results are marked in bold.

proposed method are applied to the binary image deblurring problem. We show the restoration images of "QR code" under the defocus blur and 2% noise level in Figs. 7(b)–7(d) while the restoration images of "ruler" under the motion blur and 3% noise level in Figs. 8(b)–8(d). After a visual inspection of the restored images, it is easy to check that the proposed approach yields better results than the AM and SR methods.

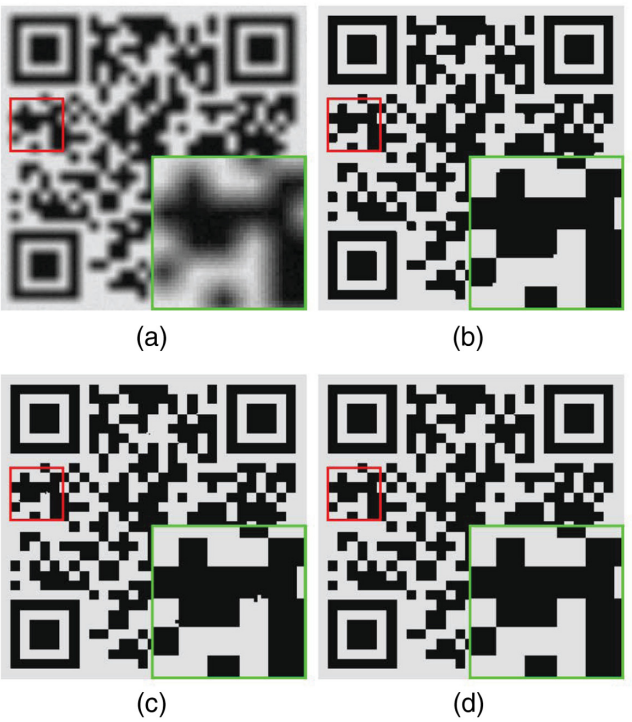

Fig. 7 Restoration results for known binary pixel values (defocus 2% noise). (a) Degraded, (b) AM,[20] (c) SR,[21] and (d) ours.

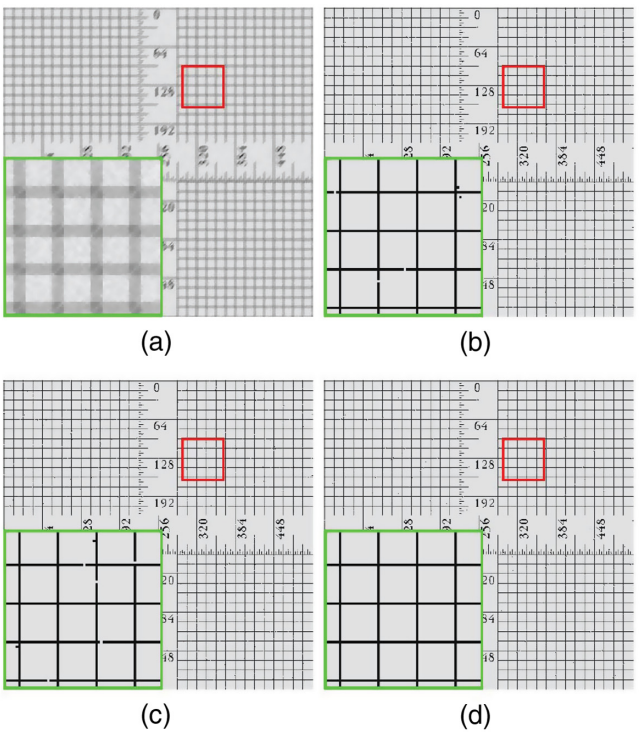

Fig. 8 Restoration results for known binary pixel values (motion, 3% noise). (a) Degraded, (b) AM,[20] (c) SR,[21] and (d) ours.

5 Conclusion

In conclusion, we propose a TV and binary constraint-based variational method with automatic binary value estimation for binary image deblurring. The numerical experiments

on binary images demonstrate the effectiveness of the proposed method. In future work, we will consider the convergence property of the related algorithms for the nonconvex optimization problem. Moreover, we will extend the proposed method to deblur pattern images which takes more than two pixel values.

Acknowledgments

This work was supported by NSFC (11671002, 61731009, 61401172, 11573011, 61601194), Nature Science Foundation of Jiangsu Province (SBK2018020024), Science and Technology Commission of Shanghai Municipality (13dz2260400), Jiangsu Key Lab for NSLSCS (201806), Qing Lan Project and Hai Yan Project, Lianyungang 521 project, and NSF of HHIT (Z2015004, Z2017004).

References

1. C. R. Vogel, *Computational Methods for Inverse Problems*, Vol. **23**, SIAM, Philadelphia, Pennsylvania (2002).
2. T. F. Chan and J. J. Shen, *Image Processing and Analysis: Variational, PDE, Wavelet, and Stochastic Methods*, SIAM, Philadelphia, Pennsylvania (2005).
3. P. C. Hansen, J. G. Nagy, and D. P. O'leary, *Deblurring Images: Matrices, Spectra, and Filtering*, Vol. **3**, SIAM, Philadelphia, Pennsylvania (2006).
4. M. K. Ng and J. Pan, "Weighted Toeplitz regularized least squares computation for image restoration," *SIAM J. Sci. Comput.* **36**(1), B94–B121 (2014).
5. X. Lv, F. Li, and T. Zeng, "Convex blind image deconvolution with inverse filtering," *Inverse Prob.* **34**(3), 035003 (2018).
6. L. I. Rudin, S. Osher, and E. Fatemi, "Nonlinear total variation based noise removal algorithms," *Physica D* **60**(1–4), 259–268 (1992).
7. Y. Lou et al., "A weighted difference of anisotropic and isotropic total variation model for image processing," *SIAM J. Imag. Sci.* **8**(3), 1798–1823 (2015).
8. M. Mignotte, "A non-local regularization strategy for image deconvolution," *Pattern Recognit. Lett.* **29**(16), 2206–2212 (2008).
9. X. Zhang et al., "Bregmanized nonlocal regularization for deconvolution and sparse reconstruction," *SIAM J. Imag. Sci.* **3**(3), 253–276 (2010).
10. J.-F. Cai et al., "Image restoration: total variation, wavelet frames, and beyond," *J. Am. Math. Soc.* **25**(4), 1033–1089 (2012).
11. X.-G. Lv, Y.-Z. Song, and F. Li, "An efficient nonconvex regularization for wavelet frame and total variation based image restoration," *J. Comput. Appl. Math.* **290**, 553–566 (2015).
12. D. Krishnan and R. Fergus, "Fast image deconvolution using hyper-Laplacian priors," in *Proc. of the 22nd Int. Conf. on Neural Information Processing Systems*, Vancouver, British Columbia, pp. 1033–1041 (2009).
13. L. Xu, S. Zheng, and J. Jia, "Unnatural L0 sparse representation for natural image deblurring," in *Proc. of the IEEE Conf. on Computer Vision and Pattern Recognition*, Portland, Oregon, pp. 1107–1114 (2013).
14. L. Chen et al., "Non convex compressive video sensing," *J. Electron. Imaging* **25**(6), 063003 (2016).
15. E. Y. Lam, "Blind bi-level image restoration with iterated quadratic programming," *IEEE Trans. Circuits Syst. Express Briefs* **54**(1), 52–56 (2007).
16. G. Y. Van et al., "A regularization approach to blind deblurring and denoising of RQ barcodes," *IEEE Trans. Image Process.* **24**(9), 2864–2873 (2015).
17. S. Esedoglu, "Blind deconvolution of bar code signals," *Inverse Prob.* **20**(1), 121–135 (2004).
18. Y. Shen, E. Y. Lam, and N. Wong, "Binary image restoration by positive semidefinite programming," *Opt. Lett.* **32**(2), 121–123 (2007).
19. J. Pan et al., "L0-regularized intensity and gradient prior for deblurring text images and beyond," *IEEE Trans. Pattern Anal. Mach. Intell.* **39**(2), 342–355 (2017).
20. J. Zhang, "An alternating minimization algorithm for binary image restoration," *IEEE Trans. Image Process.* **21**(2), 883–888 (2012).
21. X. Mei et al., "Improving image restoration with soft-rounding," in *Proc. of the IEEE Int. Conf. on Computer Vision*, pp. 459–467 (2015).
22. T. H. Li and K. S. Lii, "Deblurring two-tone images by a joint estimation approach using higher-order statistics," in *Proc. of the IEEE Signal Processing Workshop on Higher-Order Statistics*, Banff, Alberta, pp. 108–111 (1997).
23. G. Aubert and P. Kornprobst, "Mathematical problems in image processing: partial differential equations and the calculus of variations," in *Applied Mathematical Sciences*, Vol. **147**, Springer Science & Business Media, New York (2006).
24. S. Boyd et al., "Distributed optimization and statistical learning via the alternating direction method of multipliers," *Found. Trends Mach. Learn.* **3**(1), 1–122 (2010).
25. J.-F. Cai, S. Osher, and Z. Shen, "Linearized Bregman iterations for compressed sensing," *Math. Comput.* **78**(267), 1515–1536 (2009).
26. T. Goldstein and S. Osher, "The split Bregman method for L1-regularized problems," *SIAM J. Imag. Sci.* **2**(2), 323–343 (2009).
27. Z. Wang et al., "Image quality assessment: from error visibility to structural similarity," *IEEE Trans. Image Process.* **13**(4), 600–612 (2004).

Xiao-Guang Lv received his MSc and PhD degrees in mathematics from the University of Electronic Science and Technology of China, in 2007 and 2011, respectively. Since 2014, he has been an assistant professor with the School of Science, Huaihai Institute of Technology, Lianyungang, Jiangsu. His research interests include scientific computation, numerical linear algebra, inverse and ill-posed problems, and numerical optimization algorithms for image processing.

Fang Li received her MSc degree in mathematics from the South West China Normal University in 2004 and received her PhD in mathematics from East China Normal University in 2007. She worked in the Department of Mathematics in East China Normal University from 2007 and currently she is a professor. Her research interests include variational methods, optimization, and deep-learning methods in image processing.